

# FloodRISE Mapping Methods for the Tijuana River Valley and Goat Canyon Watershed

Adam Luke\*, Brett Sanders\*

---

## Abstract

The FloodRISE hazard maps produced for the Tijuana River Valley and the Goat Canyon Watershed resulted from three distinct tasks: flood frequency analysis (FFA), hydrologic and hydraulic modeling, and post-processing of model output. Generally speaking, FFA estimates the recurrence interval of rare flooding events, while hydrologic and hydraulic modeling predicts the hazards associated with simulated floods (depths, velocities, extents, etc.). Several of the produced maps required post-processing methods to combine the results of multiple simulations into a single mapping product. This document outlines the FFA, hydraulic modeling, and post-processing methods that were applied by FloodRISE to produce the Tijuana River Valley and Los Laureles flood hazard maps. The sources of the qualitative legend descriptions are also provided.

---

## 1. Flood Frequency Analysis

FFA is complicated in the coastal zone due to the multiple causes or “drivers” of flooding. Figure 1 shows the broader geographic context of the Tijuana River Estuary and demonstrates the susceptibility of estuarine environments to multiple flood drivers. In this study, we mapped flooding caused by extreme ocean levels, stream flow from the Tijuana (TJ) River, and precipitation over Goat Canyon and Smuggler’s gulch watersheds. The presence of multiple flood drivers often warrants a multivariate approach for FFA [13]. Under this approach, multivariate extreme value analysis (EVA) is used to estimate the probability of scenarios where multiple extremes occur simultaneously. However, we did not conduct multivariate EVA in this study because of the low correlation between flood drivers and the lack of emergent flood hazards caused by the joint occurrence of extremes.

Table 1 presents the Pearson’s correlation coefficient matrix between the flood drivers considered herein. The relatively low correlation is somewhat surprising but understandable. Extended periods of above average rainfall in the upper TJ River Watershed cause large stream flow events, whereas relatively short-lived coastal storm systems can elevate ocean water levels and lead to intense precipitation. The low correlation between flood drivers demonstrates that the simultaneous occurrence of extreme events would be especially rare. Perhaps more importantly, hydraulic model sensitivity analysis revealed that predicted flood depths, extents, and velocities are insensitive to the joint-occurrence of extremes in this system. For example, flood depths predicted by the hydraulic model are not sensitive to the downstream ocean level during large TJ River floods. The lack of “sufficient” correlation between drivers and the hydraulic model’s insensitivity to the joint occurrence of extremes

allows us to consider the flood drivers independently and use univariate EVA for frequency analysis.

### 1.1. Tijuana River Flood Frequency Analysis

FFA of TJ River flows was based on a Pearson Type III (PIII) distribution fitted to the historic record of log-transformed annual maximum discharges. This approach is consistent with the recommended FFA methodology in the US [17]. The data record originated from TJ River flow measurements at the US/ME border reported by the International Boundary and Water Commission. To infer the parameters of the PIII distribution, we used the Bayesian parameter estimation technique described by Luke et al. [7] where an informative prior was used to incorporate regional information about the skewness of the PIII distribution. For the TJ River, parameter estimation was complicated by signs of nonstationarity in the historic record, or time variant statistical properties of the annual maximum discharge data.

Figure 2A shows the full data record at the US/ME border. At the time of this study, data was not available after 2006. The *black* line in Figure 2A denotes the year when the TJ River channelization was completed, which appeared to alter the mean and standard deviation of the flood peaks. Indeed, the pre-channelization distribution is different from the post-channelization distribution at the 0.05 significance level according to the two-sample Kolmogorov-Smirnov test [9]. Due to the apparent change in the distribution of flood peaks following channelization, we did not use data prior to 1979 for estimation of the PIII parameters. The choice to omit data prior to channelization creates a relatively small sample size for parameter estimation and leads to large variance in the estimated return periods (Figure 2B). Assuming stationarity following the channelization, the return periods in Figure 2B are simply the inverse of the annual exceedance probabilities associated with the return levels on the y axis. If the pre-channelization flood peaks are included in the frequency analysis, we risk bias in the parameter estimates and resulting return periods.

Notice also that the empirical frequency curve shown in

---

\*Department of Civil and Environmental Engineering, University of California, Irvine

Email addresses: aluke1@uci.edu (Adam Luke), bsanders@uci.edu (Brett Sanders)

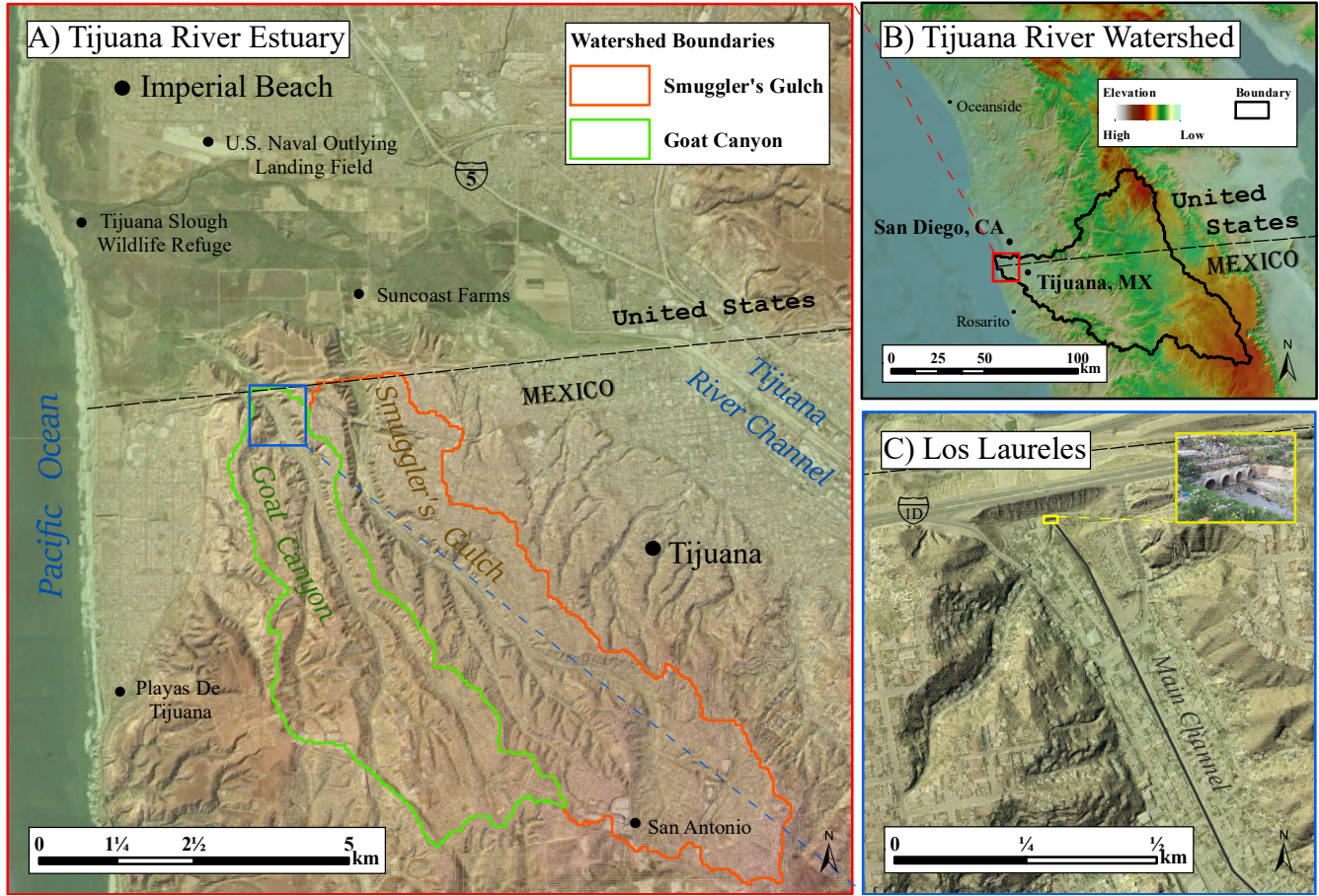


Figure 1: A) Tijuana River Estuary and relevant features. The Estuary is bounded by Imperial beach to the North and the US/Mexico Border to the South. Discharges from the Tijuana River channel enter the river valley near the US/ME Border. B) Tijuana River Watershed and broader geographical context. Notice the international aspect of the Watershed; about one third of the Watershed area is within the US, and the rest is within Mexico. C) Los Laureles community and Goat Canyon main channel. The culvert is also shown, which conveys storm water discharges from the channelized section of the Goat Canyon stream network.

Figure 2B appears to change shape near the 5 year return period level. We attribute this to the considerable influence of upstream reservoirs on large TJ River flows. Spillway discharges occurred during four of the annual maximum events from 1979 - 2006, but did not affect the majority of the relatively small, run-off driven annual maximum events. The various flood generating mechanisms and the change in the shape of the empirical frequency curve both indicate that the distribution of flood peaks is not the same for small and large annual maximum events. This causes a poor fit of the PIII distribution to the data in the modern period of record and creates even more variance in the frequency estimates. It is unlikely that the variance can be significantly reduced without expanding the sample size through watershed modeling and simulation of peak flows, which was outside the scope of this study. It is very important to note that exceedance probabilities and corresponding frequency estimates based on the historic TJ River discharges alone are unavoidably uncertain.

### 1.2. Extreme Ocean Level Frequency Analysis

Extreme ocean levels near the TRV also showed signs of nonstationarity in the historic data record. Figure 4 shows the annual maximum compared to the annual mean ocean levels

recorded at the La Jolla tide gage in CA, US. There is a statistically significant trend in both the annual maximum and mean data at the 0.05 significance level, according to the Man-Kendall trend test for monotonic trends [8, 6]. The persistent trend in ocean levels is not surprising, however it does complicate EVA. In this study, we explicitly modeled the change in extreme ocean levels using a nonstationary, generalized extreme value (GEV) distribution

$$X \sim \text{GEV}(\mu_t, \sigma, \xi) \quad (1)$$

where the random variable  $X$  is the annual maximum ocean level, and  $\sigma$  and  $\xi$  denote the scale and shape parameter of the GEV distribution, respectively. The time-variant location parameter,  $\mu_t$ , is formulated as a function of changes in mean sea level

$$\mu_t = \Delta\text{MSL}_o + \mu_o \quad (2)$$

where  $\Delta\text{MSL}_o$  is the change in annual mean sea level relative to the mean during the 1983 - 2001 tidal epoch, and  $\mu_o$  is a constant off-set between the location of the GEV distribution and mean sea level. This model was proposed by Obeysekera and Park [10] to provide a method for synthesizing extreme value

Table 1: Pearson’s correlation coefficient matrix between the three drivers of flooding considered in this study. The numeric values in the table describe the correlation between the variables in the row and column headings. Correlation coefficients were determined using de-trended tide gage data at La Jolla (NOAA station 9410230), precipitation measurements from the San Diego International Airport (NOAA network ID GHCND:USW00023188), and TJ River stream flow measurements at the US/ME border recorded by the International Boundary and Water Commission.

	Ocean Level (daily mean)	TJ Stream flow (daily mean)	Precipitation (24 hr sum)
Ocean Level (daily mean)	1	0.12	0.21
TJ Stream flow (daily mean)	0.12	1	0.17
Precipitation (24hr sum)	0.21	0.17	1

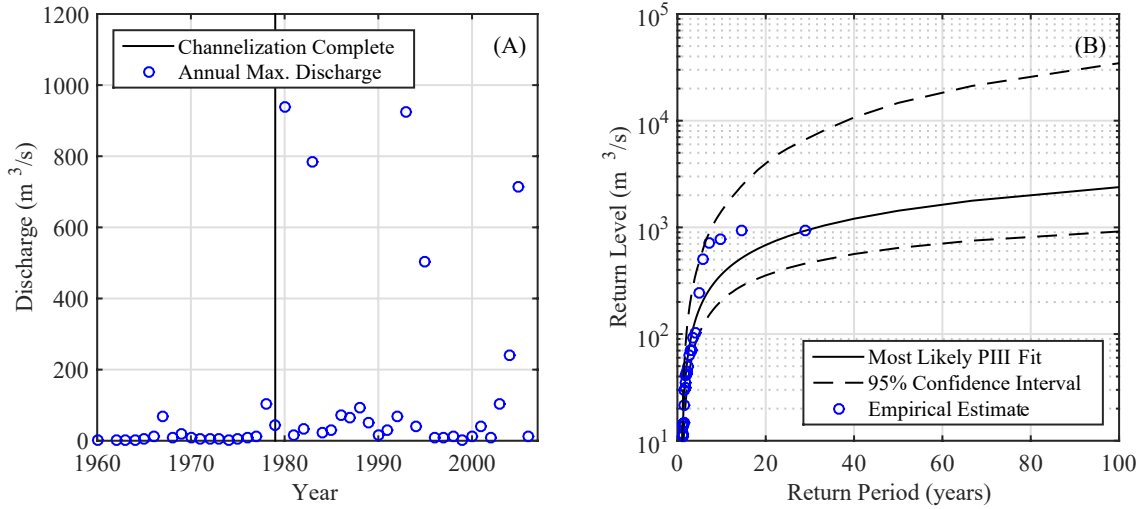


Figure 2: A) Annual maximum discharge record of the TJ River. Only flood peaks post-channelization were used for PIII parameter inference. B) Flood frequency estimates derived from the PIII distribution fitted to the log-transformed discharge data from 1979 - 2006. Notice the large variance in flood frequency estimates.

statistics with sea level rise scenarios. We estimated the parameters of the GEV model using Bayesian parameter inference, again with an informative prior on the shape parameter,  $\xi$ . The prior on  $\xi$  was specified as a normal distribution centered at the La Jolla gage estimate of  $\xi$  reported by Zervas [20]. Following parameter estimation, exceedance probabilities of extreme ocean levels are estimated as a function of change in mean sea level.

Figure 4B shows extreme water levels versus exceedance probabilities obtained from the fitted GEV model in the year 2015. Notice that along the  $x$  axis, we no longer use return periods to describe the frequency of extreme ocean levels. The common definition of a return period relies on the assumption that exceedance probabilities are time-invariant, which is very unlikely due to anticipated changes in future mean sea level. For our hazard mapping purposes, we used the nonstationary model to estimate the exceedance probabilities of extreme ocean levels associated with present day mean (2015) sea level. The fitted model could also be used to estimate exceedance probabilities associated with future sea levels by using sea level rise projections to define  $\Delta\text{MSL}_0$ .

### 1.3. Precipitation Frequency Analysis

Precipitation frequency estimates over the Goat Canyon and Smuggler’s Gulch catchments were obtained from isopluvial maps reported by Sholders [16]. The isopluvial maps provide

6 hour and 24 hour rainfall depths associated with different return periods. Rainfall depth and frequency estimates were taken from the isopluvial lines nearest to Smuggler’s Gulch and Goat Canyon catchments. To summarize and conclude the results of our frequency analysis, Table 2 includes the magnitude (return level) and exceedance probabilities for the three drivers of flooding considered herein. The values in Table 2 were used as model forcing for the hydrologic and hydraulic modeling.

## 2. Hydrologic and Hydraulic Modeling

In this study, hydrologic modeling was conducted to transform the precipitation totals over the Goat Canyon and Smuggler’s Gulch catchments (hereafter referred to collectively as “the catchments”) into flood hydrographs for input to the hydraulic models. Two hydraulic models were developed in this study: one covering the spatial extent of the Goat Canyon catchment, and the other including the Tijuana River Valley.

### 2.1. Hydrologic Modeling

The hydrologic models for the catchments were developed using (1) the Soil Conservation Service (SCS) curve number method to characterize precipitation losses from interception and infiltration [11], (2) the SCS unit hydrograph method to transform excess precipitation into a hydrograph [1], and (3) a 24-hour nested storm hyetograph (based on the totals in Table

Table 2: Most likely estimates of exceedance probabilities associated with extreme ocean levels, TJ Stream flow, and precipitation. These values were used as boundary conditions for the hydrologic and hydraulic modeling.

AEP (2015)	Ocean Level (m, NAVD88)	TJ Stream flow (m <sup>3</sup> /s)	Precipitation (24 hr sum, mm)
0.01	2.42	2333	101.6
0.02	2.40	1420	88.9
0.05	2.38	688	81.3
0.10	2.36	369	63.5
0.20	2.34	178	50.8

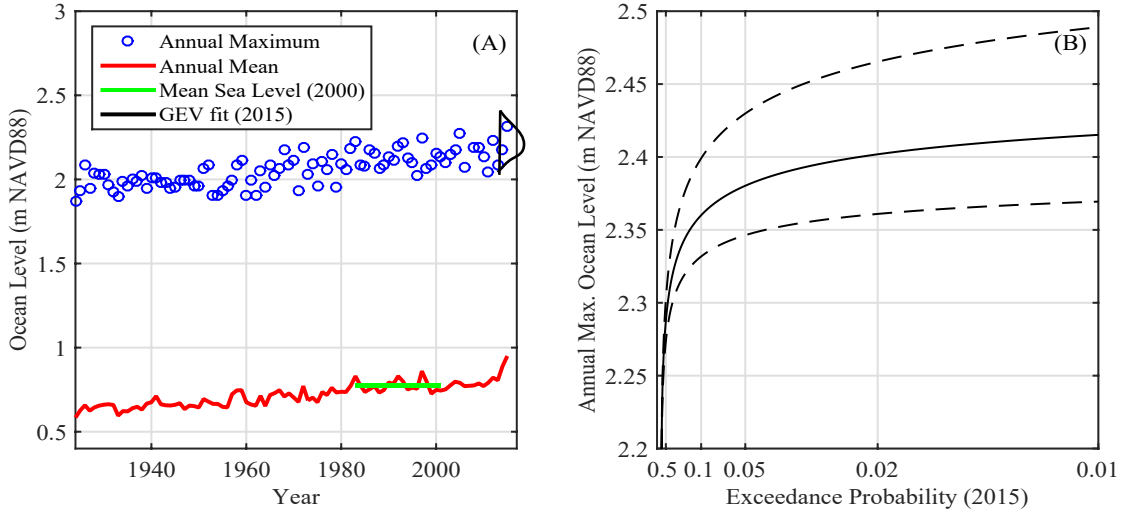


Figure 3: A) Annual maximum ocean levels compared to annual mean ocean levels recorded at the La Jolla tide gage in CA, US. The black line shows the fitted nonstationary GEV distribution during the year 2015. B) Exceedance probabilities of extreme ocean levels derived from the 2015 GEV distribution. We do not show return periods on the x axis because exceedance probabilities are expected to change as mean sea level increases.

2) to define the rainfall distribution within the 24-hour simulation [16]. The channel flow within the catchments was routed between sub-basins using the kinematic wave model described by USACE [18]. Watershed areas, channel geometries, and basin slopes were estimated from a digital elevation model (DEM) with a 0.76 m (2.5 ft) horizontal resolution, which originated from a 2014 liDAR Survey conducted by the County of San Diego. Curve numbers were defined based on land use data from the University of Arizona Remote Sensing Center and literature values from USACE [18]. Unfortunately, flow measurements within or at the catchment outlets were not available at the time of the study, so hydrologic model calibration was not possible.

## 2.2. Goat Canyon Hydraulic Model

For mapping purposes, flows in Goat Canyon were routed using BreZo [14], which solves the shallow water equations using a 2D finite volume scheme optimized for applications involving natural topography. BreZo operates on an unstructured grid of triangular or quadrilateral cells, which allows for variable mesh resolution and geometries throughout the modeling domain. The Goat Canyon modeling domain covers the entire area of the Goat Canyon Watershed (Figure 1), with an average cell area of 13.4 m<sup>2</sup>. The Goat Canyon mesh was generated using Gmsh [5] to create a structured, quadrilateral grid along channels and a mixed-mesh of triangular and quadrilateral cells

in the floodplain. The structured, quadrilateral portion of the mesh was aligned with trapezoidal channels and small gutters along streets within Goat Canyon. We used GPS measurements of channel bank and bottom elevations to define the elevation of mesh nodes aligned with channels. Mesh node elevations within the floodplain were based on the DEM from the 2014 liDAR Survey. Resistance was characterized using spatially-varying Manning's n values, where a value of 0.015 s/m<sup>(1/3)</sup> was used for concrete surfaces, and 0.035 s/m<sup>(1/3)</sup> was used for natural areas of the floodplain. Again, no flow or stage measurements existed within Goat Canyon at the time of the study, so the hydraulic model is un-calibrated.

## 2.3. Tijuana River Valley Hydraulic Model

Tijuana River Valley (TRV) flows were also routed using BreZo [14]. The TRV mesh was generated using Triangle [15], resulting in a triangular mesh of variable resolution throughout the modeling domain. The mesh domain is bounded by the Pacific ocean to the West, Imperial Beach to the North, and the elevated terrain near the US/ME border to the South (Figure 1). Mesh edges were aligned with the TJ River channel banks and small levee systems found within the TRV. The resolution of the mesh is highly variable; cells overlapping small channels in the Estuary were assigned an area of 36 m<sup>2</sup>, whereas relatively homogeneous regions in the floodplain were assigned a cell area of 100 m<sup>2</sup>. Mesh node elevations within the floodplain were

also based on the DEM from the 2014 liDAR Survey. Flow resistance was characterized using spatially varying Manning’s  $n$  values, where the Manning’s  $n$  value was determined based on land use data. Values ranged from  $0.011 \text{ s/m}^{(1/3)}$  within the TJ River channel to  $0.1 \text{ s/m}^{(1/3)}$  for densely vegetated, riparian areas.

The TRV hydraulic model was validated using observations of water surface elevations in the Estuary and the TJ River at the US/ME border. Observations of Estuary water levels and TJ River stage were obtained from the National Estuarine Research Reserve System and the International Boundary and Water Commission, respectively. In the TJ River channel, comparison of modeled stage to observed stage yielded a root mean square error of  $0.25 \text{ m}$  for TJ river flow rates of  $0 - 1040 \text{ m}^3/\text{s}$ . The error in modeled water surface elevations is most likely due differences in the sediment level in the TJ channel between the observed and modeled events. To validate the downstream region of the TRV model, we simulated a 2-week tidal cycle at the ocean boundary and compared modeled water surface elevations to those observed during the same 2-week period. Over the 2 week period, the root mean square error between observed and modeled water surface elevations was  $0.07 \text{ m}$ . The error in modeled water surface elevations in the Estuary is within the error of the topographic data. Thus, the TRV hydraulic model accurately reproduces water surface elevations for both riverine and tidal forcing.

#### 2.4. Hydraulic Model Forcing

Developing hydraulic modeling scenarios appropriate for hazard mapping requires careful consideration. For the TRV hydraulic model, the presence of multiple flood drivers complicates the development of scenarios that represent the exceedance probabilities in Table 2. This is not an issue for the Goat Canyon hydraulic model, since only one driver of flooding was considered in Goat Canyon. From a hazard mapping perspective, the challenge in Goat Canyon is coupling the hydrologic model with the hydraulic model. Our approaches for addressing both of these issues are outlined in this section.

In this study, the Goat Canyon hydraulic model was coupled with the hydrologic model differently before and after stakeholder consultations. Prior to the stakeholder consultations, the hydrographs generated by the hydrologic model described in Section 2 were input to the Goat Canyon hydraulic model as point-sources of discharge at the sub-watershed outlets within the hydrologic modeling domain. Under this approach, all effective runoff reaches the storm water channels without explicit routing of the stormwater in the out-of-bank areas. This is not ideal for hazard mapping because only areas susceptible to channel overtopping appear on the hazard map. After stakeholder consultations, we added the effective precipitation directly to the 2D modeling grid. We used the SCS curve number method to estimate the effective precipitation from the rainfall hyetographs, where each 2D model cell was assigned a curve number based on land-use. The effective rainfall hyetographs were added to the 2D grid as spatially distributed sources of discharge. Flow was routed for partially wet cells using kinematic

wave theory with the friction slope approximated using Manning’s equation, whereas flow was routed using the 2D shallow water equations for fully-wetted cells. Explicit routing of the stormwater flows results in the final hazard maps presented online. Maps produced using the former method are not shown.

To address the issue of multiple flood drivers in the TRV, we simulated the extreme conditions of each driver separately with the TRV hydraulic model. It is important to note that if multiple extremes are modeled simultaneously, for example a scenario where an abnormal ocean level coincides with an extreme TJ River flood, the resulting flood hazard would not be associated with the exceedance probabilities of the individual events. Thus, during the TJ River flood simulations, the downstream (ocean) boundary conditions were defined as mean-tidal cycles, and the flows from the catchments were set to zero. To define the the TJ River flow hydrographs, we scaled the hydrograph associated with the 1980 flood to the peak discharges in Table 2. These scaled hydrographs served as boundary conditions at the upstream boundary of the modeling domain. The resulting TJ river flood hazards predicted by the hydraulic model are therefore associated with the exceedance probabilities defined in Table 2. The extreme ocean level simulations were developed using the same reasoning. An average, 12-hour tidal cycle was scaled to the extreme ocean levels in Table 2 to define the ocean boundary of the model. During the extreme ocean level simulations, flows from the catchments and the TJ River were set to zero. Lastly, for the extreme precipitation scenarios, the hydrographs predicted by the hydrologic model associated with the rainfall events in Table 2 were input as point sources to the hydraulic model at the catchment outlets (Figure 1). During these simulations, the ocean boundary conditions were defined as mean-tidal cycles, while the flows from the TJ River were set to zero. This approach results in an ensemble of hydraulic model output that is a function of 1) exceedance probability and 2) flood drivers. We combined the results of these simulations into hazard maps using probability rules and post-processing techniques.

### 3. Post-Processing Methods

For each hydraulic model simulation, we saved the cell-centered maximum flood depths, unit discharges, depth averaged shear stresses, and durations of depth greater than  $0.11 \text{ m}$ . These “hazard variables”, denoted collectively as  $H$ , were processed following simulation to produce the various hazard maps. To create a continuous raster surface from the discrete  $H$  values of the hydraulic model cell-centers, we used an inverse distance weighted interpolation scheme. The continuous raster surfaces are the mapped hazard data shown in this study. The Los Laureles hazard maps of  $H$  required no further post-processing, since only one driver was considered. However, for the TRV hazard maps, we contoured the maximum value between the three different drivers of flooding

$$\mathbb{H}_i = \max(\{H_i^A, H_i^B, H_i^C\}) \quad (3)$$

where  $\mathbb{H}_i$  is the mapped hazard value at raster surface location  $i$ , and the superscripts  $A$ ,  $B$ , and  $C$  denote  $H$  values resulting from

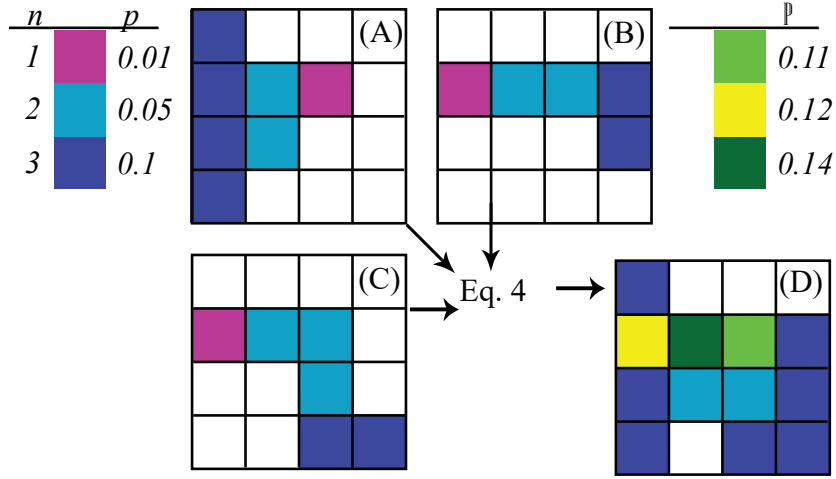


Figure 4: Illustration of methodology for mapping the exceedance probability of a hazard threshold from multiple flood drivers. A) Raster of  $P_i^A$  values for generic flood driver, A. B) Raster of  $P_i^B$  values for generic flood driver, B. C) Raster of  $P_i^C$  values for generic flood driver, C. D) Exceedance probability raster of  $\mathbb{P}_i$  values resulting from flood driver A, B, or C.

extreme ocean level, TJ river flow, and extreme precipitation simulations, respectively.  $H_i^A$ ,  $H_i^B$ , and  $H_i^C$  are associated with the same exceedance probabilities when combined in this manner. The TRV hazard maps therefore depict flood hazards with specific exceedance probabilities resulting from either driver of flooding considered, depending on location within the TRV.

The maps contouring the exceedance probabilities of specific flood hazard thresholds required additional processing. First, raster surfaces of exceedance probability  $P_i$  were created for each flood driver considered. Given a set of hydraulic model output corresponding to  $n$  exceedance probabilities,  $p_1, p_2, \dots, p_n$ , the exceedance probability at raster location  $i$  is given by the largest value of  $p$  for which the hazard level  $H_i$  exceeds a prescribed threshold. To account for the three drivers of flooding in TRV, three probability raster surfaces were computed:  $P_i^A$ ,  $P_i^B$  and  $P_i^C$ , which denote the probability of exceeding the hazard threshold from extreme ocean levels, TJ river floods, and extreme precipitation, respectively. Next, based on the assumption of independence between drivers, the mapped probability is given by

$$\mathbb{P}_i = (P_i^A + P_i^B + P_i^C) - (P_i^A \cdot P_i^B) - (P_i^A \cdot P_i^C) - (P_i^B \cdot P_i^C) - (P_i^A \cdot P_i^B \cdot P_i^C) \quad (4)$$

where  $\mathbb{P}_i$  is the exceedance probability of the hazard threshold at location  $i$  resulting from all drivers of flooding considered. In Los Laureles,  $\mathbb{P}_i = P_i^C$  since only flooding caused by extreme precipitation was simulated. Notice that equation 4 results from probability addition rules of three independent events, and could be expanded or contracted depending on the number of flood drivers considered. Figure 4 illustrates this mapping methodology.

#### 4. Legend Descriptions

The hazard maps of flood depths, force, and shear stresses include qualitative legend descriptions. All of these qualitative descriptions are supported by previous studies. The body scales used in the depth legends are based on the average person height reported by Fryar et al. [3], with the body part thresholds defined using the 7.5 heads rule from the field of artistic anatomy [12]. The flood “force” maps are more precisely described as maps contouring the predicted flood depths multiplied by flow velocity, or the discharge per unit width. We use depth multiplied by velocity to indicate force of the flowing water because flow conditions necessary to topple people, move cars, or damage homes correlate well with the depth velocity product. In the flood “force” legends, the threshold for toppling people is based on values reported by Xia et al. [19] that represent the discharge necessary to topple people 4 ft 1 inch, 56 lbs (children). The threshold for displacing cars represents discharge necessary for Mini-Coopers to begin moving in floodwaters reported Xia et al. [19]. The thresholds for structural home damage and complete washout are equal to the best performing thresholds reported by Gallegos et al. [4], who tested the ability of discharge criteria to predict the damage states of wood-framed homes. Lastly, the shear stress map legends are based on engineering design criteria for stream restoration materials. The shear stresses necessary to erode different soil types and vegetated surfaces were taken from the values reported by Fischenich [2] and the references therein.

#### 5. Acknowledgements

This work was made possible by the National Science Foundation (grant DMS-1331611), whose support we gratefully acknowledge. We also gratefully acknowledge Professor Trent Biggs, Kristine Taniguchi, and Napoleon Elizondo for their assistance with data collection and sharing site knowledge.

## References

- [1] National Engineering Handbook Section 4 (NEH), Tech. rep., United States Department of Agriculture, Natural Resource Conservation Service, 1985.
- [2] Fischenich, C.: Stability thresholds for stream restoration materials, Tech. rep., ENGINEER RESEARCH AND DEVELOPMENT CENTER VICKSBURG MS ENVIRONMENTAL LAB, 2001.
- [3] Fryar, C. D., Gu, Q., and Ogden, C. L.: Anthropometric reference data for children and adults: United States, 2007-2010., Vital and health statistics. Series 11, Data from the national health survey, pp. 1–48, 2012.
- [4] Gallegos, H. A., Schubert, J. E., and Sanders, B. F.: Structural damage prediction in a high-velocity urban dam-break flood: field-scale assessment of predictive skill, *Journal of Engineering Mechanics*, 38, 1249–1262, 2012.
- [5] Geuzaine, C. and Remacle, J.-F.: Gmsh: A 3-D finite element mesh generator with built-in pre-and post-processing facilities, *International journal for numerical methods in engineering*, 79, 1309–1331, 2009.
- [6] Kendall, M.: Rank correlation methods, Griffin, London, 4th edn., 1976.
- [7] Luke, A., Vrugt, J. A., AghaKouchak, A., Matthew, R., and Sanders, B. F.: Predicting nonstationary flood frequencies: Evidence supports an updated stationarity thesis in the United States, *Water Resources Research*, 2017.
- [8] Mann, H.: Nonparametric tests against trend, *Econometrica*, 13, doi:10.2307/1907187, 1945.
- [9] Massey Jr, F. J.: The Kolmogorov-Smirnov test for goodness of fit, *Journal of the American statistical Association*, 46, 68–78, 1951.
- [10] Obeysekera, J. and Park, J.: Scenario-based projection of extreme sea levels, *Journal of Coastal Research*, 29, 1–7, 2012.
- [11] Ponce, V. M. and Hawkins, R. H.: Runoff curve number: Has it reached maturity?, *Journal of hydrologic engineering*, 1, 11–19, 1996.
- [12] Richer, P. M. L. P.: Artistic anatomy, Watson-Guptill Publications, 1986.
- [13] Salvadori, G. and De Michele, C.: Multivariate extreme value methods, in: *Extremes in a changing climate*, pp. 115–162, Springer, 2013.
- [14] Sanders, B. F., Schubert, J. E., and Detwiler, R. L.: ParBreZo: A parallel, unstructured grid, Godunov-type, shallow-water code for high-resolution flood inundation modeling at the regional scale, *Advances in Water Resources*, 33, 1456–1467, 2010.
- [15] Shewchuk, J. R.: Triangle: Engineering a 2D quality mesh generator and Delaunay triangulator, in: *Applied computational geometry towards geometric engineering*, pp. 203–222, Springer, 1996.
- [16] Sholders, M.: San Diego County Hydrology Manual, Tech. rep., County of San Diego, Department of Public Works, Flood Control Section, 2003.
- [17] Subcommittee, H.: Guidelines for determining flood flow frequency, *Bulletin B*, 17, 1982.
- [18] USACE: Hydrologic Modeling System HEC-HMS Technical Reference Manual, Tech. rep., 2000.
- [19] Xia, J., Falconer, R. A., Wang, Y., and Xiao, X.: New criterion for the stability of a human body in floodwaters, *Journal of Hydraulic Research*, 52, 93–104, 2014.
- [20] Zervas, C.: NOAA technical report NOS Co-OPS 067: extreme water levels of the United States 1893–2010, Tech. rep., Technical report, National Oceanic and Atmospheric Administration/National Ocean Service/Center for Operational Oceanographic Products and Services, Silver Spring, MD, 2013.